Appl. Phys. B 89, 521–526 (2007)
DOI: 10.1007/s00340-007-2871-8

Applied Physics B
Lasers and Optics

P. ROSE[1,✉]
T. RICHTER[2]
B. TERHALLE[1]
J. IMBROCK[1]
F. KAISER[2]
C. DENZ[1]

Discrete and dipole-mode gap solitons in higher-order nonlinear photonic lattices

[1] Institut für Angewandte Physik and Center for Nonlinear Science (CeNoS), Westfälische Wilhelms-Universität Münster, Corrensstraße 2, 48149 Münster, Germany
[2] Institut für Angewandte Physik, Technische Universität Darmstadt, Hochschulstraße 4a, 64289 Darmstadt, Germany

Received: 5 July 2007/Revised version: 7 November 2007
Published online: 1 December 2007 •

ABSTRACT We investigate the formation of fundamental discrete solitons and dipole-mode gap solitons in triangular photonic lattices imprinted in photorefractive nonlinear media. These lattices are strongly affected by the photorefractive anisotropy, resulting in orientation-dependent refractive index structures with reduced symmetry. It is demonstrated that two different orientations of the lattice wave enable the formation of fundamental discrete solitons in the total internal reflection gap. Furthermore, it is shown that one lattice orientation additionally supports dipole-mode solitons in the Bragg reflection gap. The experimental results are corroborated by numerical simulations using the full anisotropic model.

PACS 42.65.Tg; 42.65.Wi; 42.70.Qs

1 Introduction

Nonlinear periodic structures have recently become an active area of research due to many exciting possibilities of controlling wave propagation, steering and trapping. Periodicity changes the wave bandgap spectrum and therefore strongly affects propagation and localization, leading to the formation of discrete and gap spatial solitons which have already been studied in several branches of science [1–4].

In optics, a periodic modulation of the refractive index can either be pre-fabricated as in photonic crystals [5] or optically induced in photorefractive materials [6–9]. Until now, several different approaches for the fabrication of photonic crystals exist [10–12]. Although these mechanisms enable a precise material structuring with periodicities adequate for optical waves, they do not allow for flexible changes of structural parameters (e.g., lattice period or modulation depth). In contrast, the optical induction in photorefractive crystals provides highly reconfigurable, wavelength-sensitive nonlinear structures which can be induced at very low power levels.

It was this configuration that opened a new field of formation of discrete and gap solitons showing from the first description [9] to complex configurations and soliton scenarios as soliton trains [13], Zener tunneling [14] and even mobility investigations [15]. A concise review can be found in [16].

However, up to now, in almost all these demonstrations the optically induced lattices have been restricted to a fourfold symmetry in a diamond-like orientation. This is due to the fact that in this lattice configuration effects of the anisotropy of the electro-optic properties of photorefractive crystals can be neglected.

Recently, in the same spirit, the formation of discrete and gap solitons in hexagonal lattices (Fig. 1) has also been demonstrated [17, 18]. Again, the orientation of the lattice wave has been chosen to minimize the effect of anisotropy.

In general lattice orientations or symmetries, the induced refractive index change depends strongly on the anisotropy of the photorefractive response as well as on the polarization of the lattice wave [19–21]. In particular, its spatial orientation with respect to the *c*-axis of the crystal determines the symmetry of the resulting refractive index lattice, which can be different from the inducing light pattern.

Even when considering lattices with the fourfold symmetry as the simplest example of highly symmetric structures, two lattice orientations can already be distinguished: a square pattern with one high-symmetry axis orientated parallel to the *c*-axis, and a 45° tilted, so-called diamond pattern as it has been used in most experiments up to now. We have recently demonstrated that, due to the photorefractive anisotropy, the square lattice results in an effectively one-dimensional refractive index structure consisting of vertical lines, whereas the induced refractive index change for the diamond pattern contains well separated spots, thus forming a fully two-dimensional structure [19].

Furthermore, the anisotropic structure of the induced refractive index change has been shown to influence the symmetry of discrete solitons [21]. Due to the effectively one-dimensional refractive index modulation, the discrete solitons generated in the square lattice resemble two-dimensional solitons in a quasi one-dimensional lattice potential whereas a probe beam in the diamond lattice follows the dynamics known for truly two-dimensional lattices.

The purpose of this paper is to extend the concept of solitons in optically induced lattices to more complex anisotropic lattices and to demonstrate experimentally as well as numerically, that with a concise analysis of the non-diffracting pat-

✉ Fax: +49-251-8339811, E-mail: patrick.rose@uni-muenster.de

terns which are propagating stable in the anisotropic photorefractive material, the formation of discrete and gap solitons is possible. Thereby, we overcome previous limitations of useable lattice configurations and extend the possibilities of available lattices for soliton formation considerably.

As an example of an anisotropic photonic structure, we have chosen complex triangular lattices, due to the fact that they not only represent an example of highly-symmetric patterns that are transformed into lattices with strongly reduced symmetry, but also patterns that are an extension of the commonly known fourfold symmetry diamond or square lattices. Triangular lattices are higher-order lattices consisting of dipole structures oriented in a diamond pattern with angles of 60°.

A similar effect of symmetry reduction can also be observed for the hexagonal lattices (Fig. 1) already implemented. However, for the triangular lattices the photorefractive anisotropy leads to crucially different refractive index structures (cf. Figs. 1c and 3d as well as Figs. 1d and 4d). Certainly, this results in different bandgap spectra and hence influences the characteristics of possible solitons dramatically.

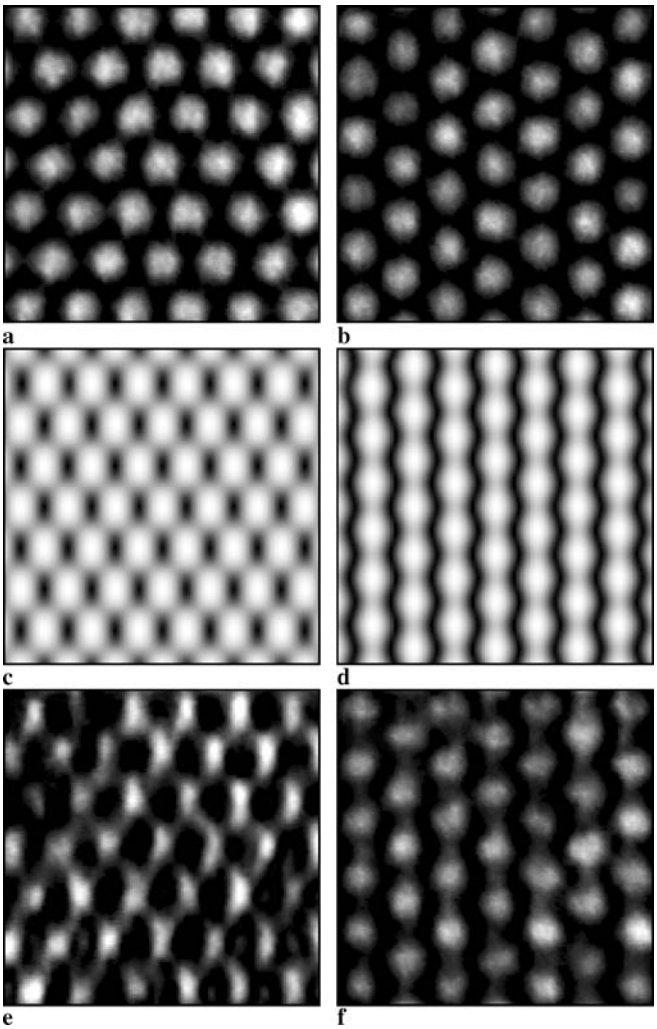

FIGURE 1 Structure analysis of the parallel (*left*) and perpendicular hexagonal pattern (*right*). (**a**, **b**) Lattice wave, (**c**, **d**) numerical simulation of the light-induced refractive index change, (**e**, **f**) guided wave

To the best of our knowledge, there exist neither theoretical nor experimental studies of soliton formation in this lattice type so far. In particular, we show that the symmetry of discrete solitons is influenced by the photorefractive anisotropy in a very similar way as in lattices with fourfold symmetry. We then expand our analysis to the propagation of dipole-modes [22] and show that the triangular lattice in parallel orientation enables the formation of dipole-mode gap solitons. This is the first demonstration of a stable dipole structure – a molecule of light – in a highly anisotropic lattice.

2 Experimental setup

The experimental setup is shown schematically in Fig. 2.

A beam from a frequency-doubled Nd:YAG laser at a wavelength of 532 nm is split into two beams with adjustable intensities by using a combination of half wave plate and polarizing beam splitter.

The transmitted beam illuminates a programmable spatial light modulator to imprint a phase modulation such that adjacent spots of the lattice wave obtain a relative phase shift of π radians. This phase modulation enables a diffraction free propagation of the lattice wave [19] necessary for the induction of two-dimensional periodic structures. The modulated beam is then imaged at the input face of a 20 mm long $Sr_{0.60}Ba_{0.40}Nb_2O_6$ (SBN:Ce) crystal by a high numerical aperture telescope. A half wave plate in front of the telescope is used to ensure the ordinary polarization of the lattice wave thus enabling its effectively linear propagation [6]. The crystal is additionally biased by an externally applied electric field and – to control the dark irradiance – uniformly illuminated with a white-light source.

The reflected beam passes a combination of polarizing beam splitter, quarter wave plate and piezo-mounted mirror to achieve incoherence to the lattice wave. A vortex mask within the optical path then creates an optical vortex with topological charge $m = +1$. A Mach–Zehnder interferometer setup is used to get interference of two vortices. Because of the penta prism instead of a simple mirror in one of the inter-

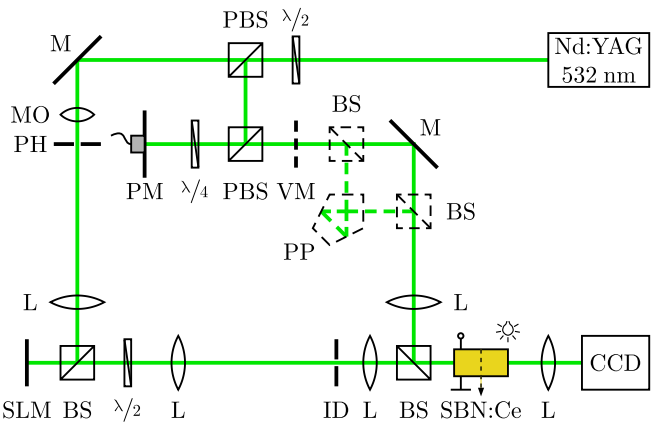

FIGURE 2 Experimental setup. CCD: camera, ID: iris diaphragm, L: lens, M: mirror, MO: microscope objective, (P)BS: (polarizing) beam splitter, PH: pinhole, PM: piezo-mounted mirror, PP: penta prism, SLM: spatial light modulator, VM: vortex mask

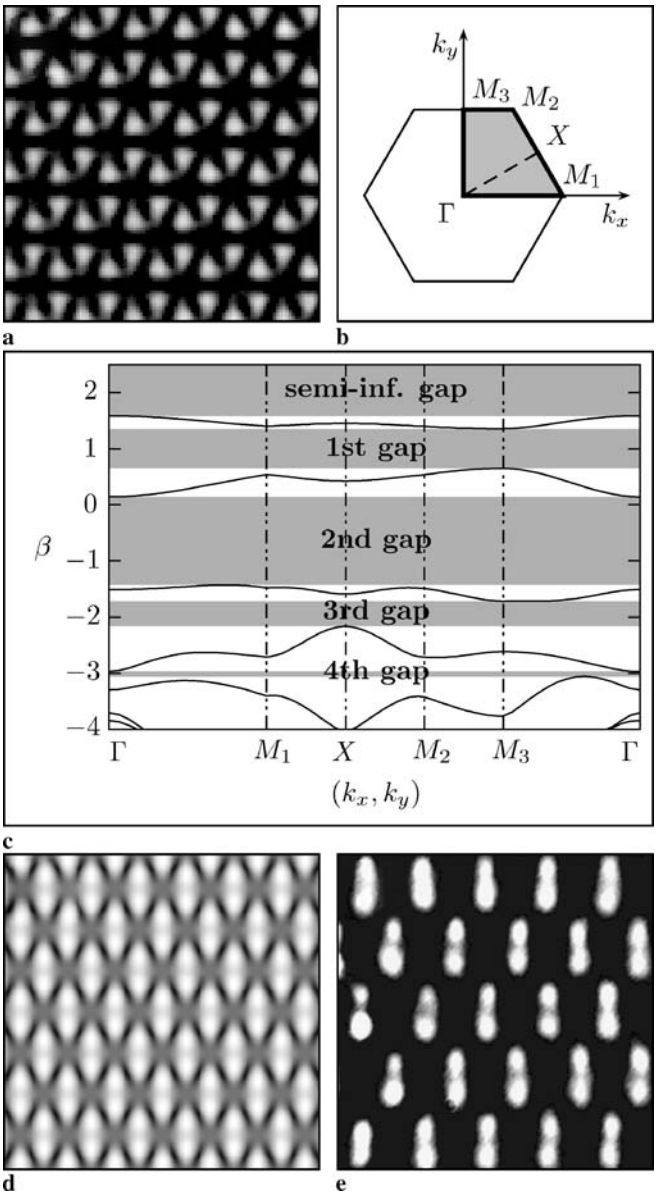

FIGURE 3 Parallel triangular pattern. (**a**) Lattice wave, (**b**) first Brillouin zone, (**c**) bandgap spectrum, (**d**) numerical simulation of the light-induced refractive index change, (**e**) guided wave

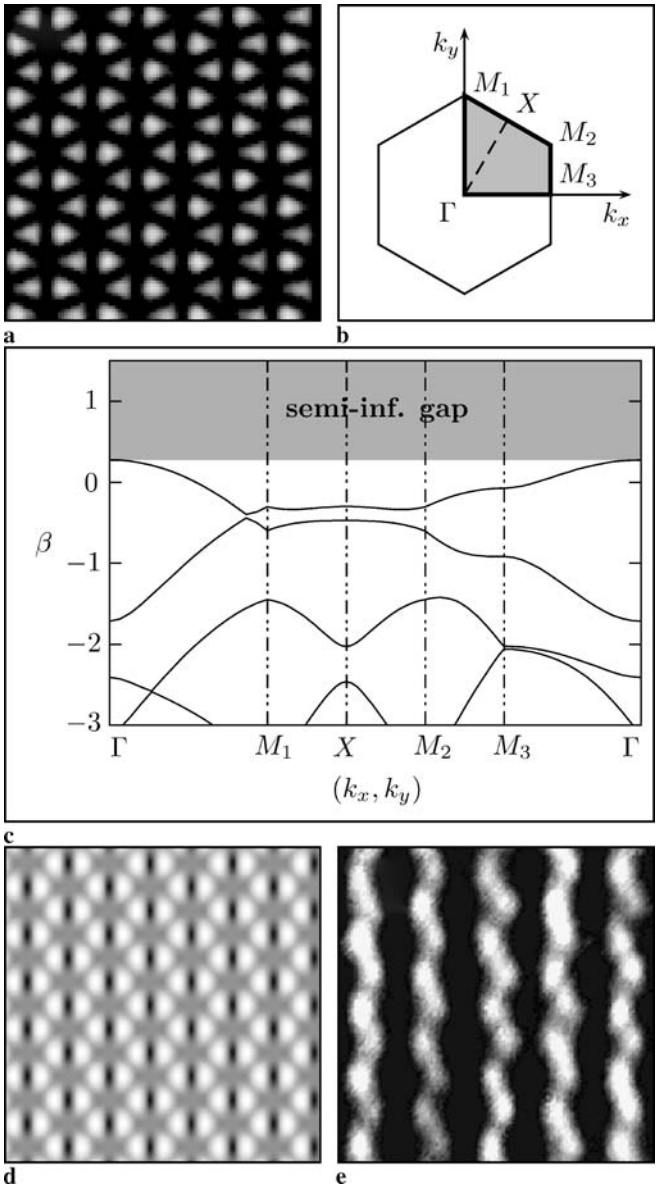

FIGURE 4 Perpendicular triangular pattern. (**a**) Lattice wave, (**b**) first Brillouin zone, (**c**) bandgap spectrum, (**d**) numerical simulation of the light-induced refractive index change, (**e**) guided wave

ferometer arms one of the interfering vortices experiences an additional reflection and therefore has a different rotational direction (topological charge $m = -1$). The interference of such counter-rotating vortices results in a dipole with a phase shift of π radians between both bright spots. The extraordinarily polarized dipole probe beam is focused onto the front face of the crystal. By removing the vortex mask, the dashed drawn beam splitters, and the penta prism (Fig. 2), the setup can be changed to use a gaussian probe beam instead of the dipole.

The output of the crystal is finally analyzed with a CCD camera.

To observe the induced refractive index structure, the lattice can be illuminated with a broad plane wave, which is then guided by the regions of high refractive index. As a consequence, the modulated intensity distribution at the output of the crystal qualitatively maps the induced refractive index change [19–21, 23]. Figure 1e and f exemplarily show the experimentally observed refractive index for the hexagonal pattern in parallel and perpendicular orientation. The experimental results are in good agreement with the numerical simulations depicted in Fig. 1c and d.

3 Triangular photonic lattices

Using the full anisotropic model [24], one can describe the optical induction of triangular lattices as well as beam propagation in these structures by the following set of equations:

$$i\frac{\partial E}{\partial z} + \nabla^2 E + \mathcal{F}(I)E = 0\,, \tag{1}$$

$$\mathcal{F}(I) = \Gamma\frac{\partial \varphi}{\partial x}\,, \tag{2}$$

$$\nabla^2\varphi + \nabla\varphi\nabla\ln(1+I) = \frac{\partial}{\partial x}\ln(1+I)\,. \tag{3}$$

It is $\nabla^2 = \partial^2/\partial x^2 + \partial^2/\partial y^2$; Γ is proportional to the electro-optic coefficient and bias dc field, φ denotes the scalar potential of the electric screening field, E is the amplitude of the extraordinarily polarized probe beam, and $I = 1 + |U|^2 + |E|^2$ gives the total light intensity, including the normalized background illumination, the lattice wave intensity $|U|^2$, and the probe beam intensity $|E|^2$.

The standard form $U(x, y, z) = \tilde{U}(x, y)\exp(\mathrm{i}\beta z)$ with

$$\tilde{U}(X, Y) = A\sin\left(\frac{2Y}{\sqrt{3}}\right)\sin\left(\frac{Y}{\sqrt{3}} + X\right)\sin\left(\frac{Y}{\sqrt{3}} - X\right)$$

leads to diffraction-free propagation of the lattice wave for the triangular patterns, where $(X, Y) = (x, y)$ for the parallel orientation (Fig. 3a) and $(X, Y) = (y, x)$ for the perpendicular orientation (Fig. 4a). In order to study the lattice induction process alone, we set $E \equiv 0$, i.e., $I = 1 + |\tilde{U}(x, y)|^2$.

Similar to the diamond and square pattern, these lattices also show strong orientation anisotropy in the symmetry of the induced refractive index changes. Corresponding numerical calculations for both lattice types are shown in Figs. 3d and 4d. For the parallel orientation (Fig. 3), every two vertically neighboring out-of-phase lobes of the field distribution induce a focusing dipole-island and these islands form essentially a diamond pattern with angles of 60° (Fig. 3d). In the same way, the triangular pattern with perpendicular orientation (Fig. 4) induces a refractive index change comparable to the square pattern with regions of high refractive index forming vertical lines (Fig. 4d) [19]. The experimentally observed guided waves (Figs. 3e and 4e) confirm these numerical results.

In order to study the formation of discrete and gap solitons in such lattices, we also calculated the bandgap spectrum for both lattice types as shown in Figs. 3c and 4c.

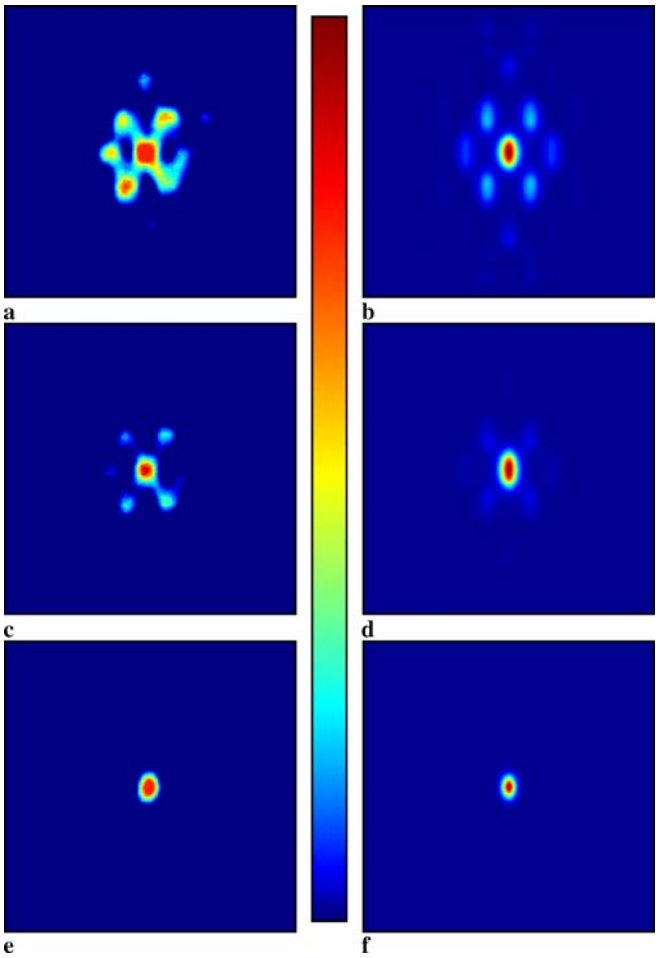

FIGURE 5 Experimental results (*left*) and numerical simulations (*right*) for the formation of fundamental discrete solitons in the parallel triangular lattice. (**a**, **b**) diffraction of the probe beam at low power (≈ 20 nW), (**c**, **d**) localized state at moderate power (≈ 45 nW), (**e**, **f**) discrete soliton (≈ 160 nW), used color map going from *blue* (low intensity) to *red* (high intensity) depicted between both *columns*

4 Fundamental discrete solitons

To describe the beam propagation in triangular photonic lattices, we also use the full anisotropic model (1)–(3). In contrast to the description of the lattice induction process, the total intensity now includes all three terms, $I = 1 + |\tilde{U}(x, y)|^2 + |E|^2$, i.e., the probe beam (soliton) intensity $|E|^2$ is no longer equal to zero. The numerical parameters are chosen to match our experimental conditions.

Experimentally, we generate fundamental discrete solitons by focusing an extraordinarily polarized gaussian beam into one lattice site at the front face of the crystal. Our results are summarized in Figs. 5 and 6 for the parallel and perpendicular lattice, respectively. Although the probe beam is extraordinarily polarized, we also observe its linear propagation (discrete diffraction) using the slow response of photorefractive nonlinearity. Indeed, the process of optical induction is much slower than the propagation of light and immediately after launching the probe beam the periodic refractive index induced by the lattice wave is undistorted.

It is clearly visible that the diffraction of the probe beam in the parallelly oriented lattice at low power shows a behavior similar to the diamond lattice, forming a fully two-dimensional diffraction pattern (Fig. 5a). In contrast, corresponding images for the perpendicular lattice (Fig. 6a) show an effectively one-dimensional diffraction pattern consisting of vertical stripes as observed for the square pattern [21].

Increasing the power of the probe beam, we observe the evolution from the described diffraction pattern to the strongly localized discrete solitons (Figs. 5e and 6e). The corresponding numerical simulations (Figs. 5 and 6, right columns) are in very good agreement with our experimental observations.

5 Dipole-mode gap solitons

In addition to the previously discussed fundamental discrete solitons in triangular photonic lattices, our numerical simulations reveal that the lattice in parallel orientation with its dipole-like islands of high refractive index gives rise to the formation of dipole-mode gap solitons originating from the M_3-point of the irreducible first Brillouin zone (Fig. 3b).

To compare these numerical simulations to the experiment, we generate a dipole-like input beam by using the superposition of two counter-rotating vortices as described in

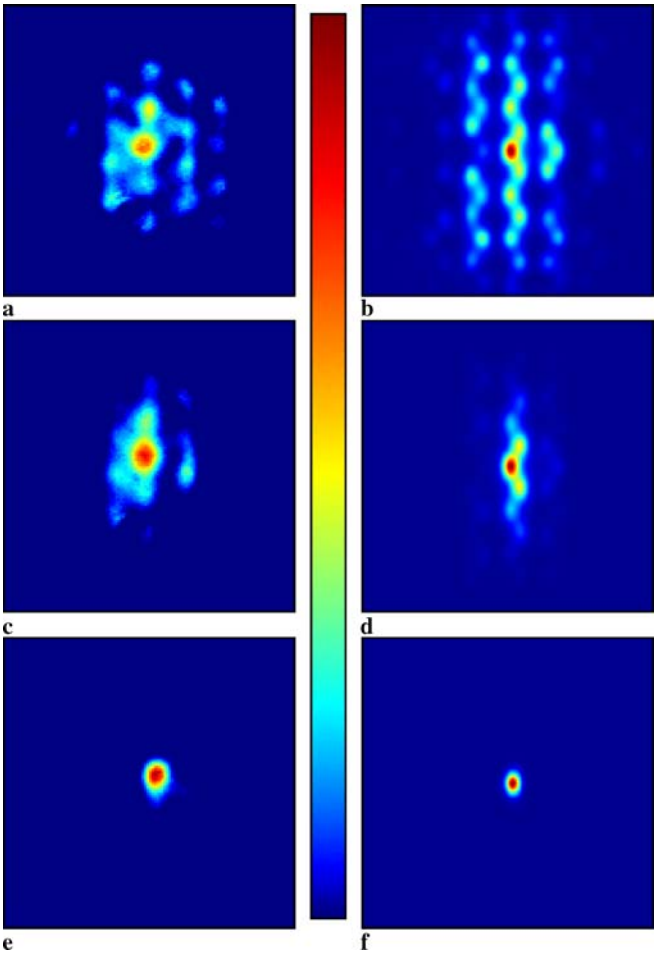

FIGURE 6 Experimental results (*left*) and numerical simulations (*right*) for the formation of fundamental discrete solitons in the perpendicular triangular lattice. (**a**, **b**) diffraction of the probe beam at low power (≈ 15 nW), (**c**, **d**) localized state at moderate power (≈ 35 nW), (**e**, **f**) discrete soliton (≈ 140 nW), used color map going from *blue* (low intensity) to *red* (high intensity) depicted between both *columns*

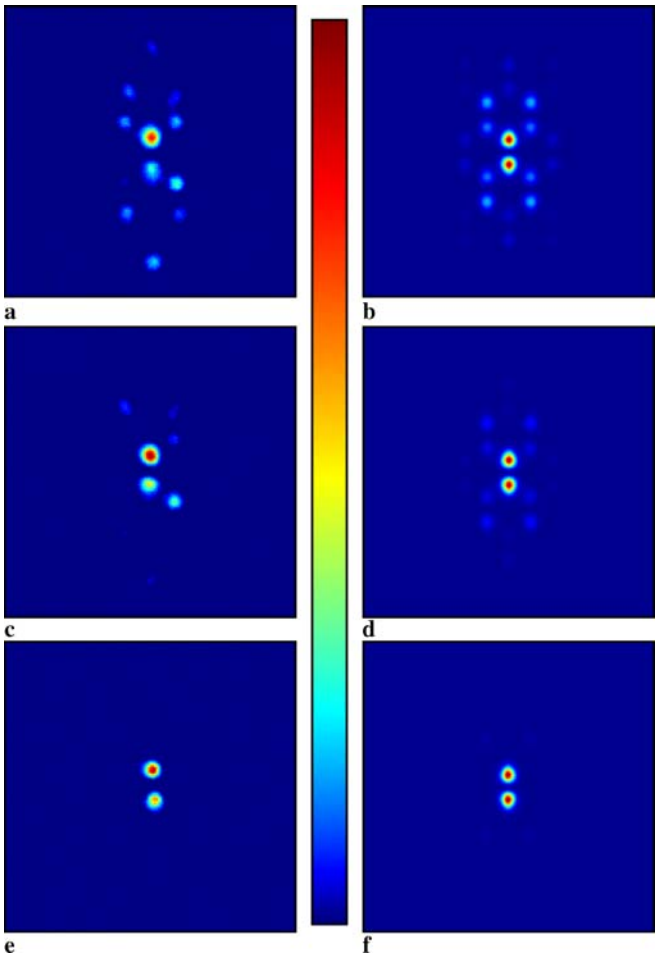

FIGURE 7 Experimental results (*left*) and numerical simulations (*right*) for the formation of dipole-mode gap solitons in the parallel triangular lattice. (**a**, **b**) diffraction of the probe beam at low power (≈ 10 nW), (**c**, **d**) localized state at moderate power (≈ 25 nW), (**e**, **f**) dipole-mode gap soliton (≈ 90 nW), used color map going from *blue* (low intensity) to *red* (high intensity) depicted between both *columns*

Sect. 2 and observe the output of the probe beam at the back face of the crystal for different probe beam powers.

The experimental as well as the numerical results are summarized in Fig. 7. At low probe beam powers the diffraction pattern consists of a central dipole surrounded by four side lobes each forming a dipole itself (Fig. 7a). With increased power the side lobes vanish and a stable dipole-mode gap soliton evolves (Fig. 7e). Again there is a very good agreement between experimental results and numerical simulations.

The existence of these stable solitons in triangular lattices offers novel possibilities to control dipole-like beams. In bulk photorefractive media they are known to experience strong repulsion [25], whereas in the presence of the lattice they are confined in one dipole-like island of high refractive index.

6 Conclusions

In conclusion, we have presented the first experimental and numerical investigation of fundamental discrete solitons as well as dipole-mode gap solitons in anisotropic triangular lattices of two different orientations. It has been shown that both lattice orientations enable the formation of fundamental discrete solitons. Moreover, the parallel lattice enables stable propagation of dipole beams due to the existence of dipole-mode gap solitons.

ACKNOWLEDGEMENTS The authors acknowledge fruitful discussions with Anton S. Desyatnikov, Nonlinear Physics Center, Research School of Physical Sciences and Engineering, Australian National University, Canberra, Australia.

REFERENCES

1 A.S. Davydov, J. Theor. Biol. **38**, 559 (1973)
2 W.P. Su, J.R. Schrieffer, A.J. Heeger, Phys. Rev. Lett. **42**, 1698 (1979)
3 A. Trombettoni, A. Smerzi, Phys. Rev. Lett. **86**, 2353 (2001)
4 D.N. Christodoulides, R.I. Joseph, Opt. Lett. **13**, 794 (1988)
5 Y.S. Kivshar, G.P. Agrawal, *Optical Solitons: From Fibers to Photonic Crystals* (Academic, San Diego, 2003), p. 540 ff
6 N.K. Efremidis, S. Sears, D.N. Christodoulides, J.W. Fleischer, M. Segev, Phys. Rev. E **66**, 046 602 (2002)
7 J.W. Fleischer, T. Carmon, M. Segev, N.K. Efremidis, D.N. Christodoulides, Phys. Rev. Lett. **90**, 023 902 (2003)
8 D. Neshev, E. Ostrovskaya, Y.S. Kivshar, W. Krolikowski, Opt. Lett. **28**, 710 (2003)
9 J.W. Fleischer, M. Segev, N.K. Efremidis, D.N. Christodoulides, Nature **422**, 147 (2003).

10 U. Grüning, V. Lehmann, S. Ottow, K. Busch, Appl. Phys. Lett. **68**, 747 (1996)
11 T.F. Krauss, R. De La Rue, S. Brand, Nature **383**, 699 (1996)
12 J. Serbin, A. Ovsianikov, B. Chichkov, Opt. Express **12**, 5221 (2004)
13 Z. Chen, H. Martin, E.D. Eugenieva, J. Xu, A. Bezryadina, Phys. Rev. Lett. **92**, 143 902 (2004)
14 H. Trompeter, T. Pertsch, F. Lederer, D. Michaelis, U. Streppel, A. Bräuer, U. Peschel, Phys. Rev. Lett. **96**, 023 901 (2006)
15 R. Fischer, D. Träger, D.N. Neshev, A.A. Sukhorukov, W. Krolikowski, C. Denz, Y.S. Kivshar, Phys. Rev. Lett. **96**, 023 905 (2006)
16 J.W. Fleischer, G. Bartal, O. Cohen, T. Schwartz, O. Manela, B. Freedman, M. Segev, H. Buljan, N.K. Efremidis, Opt. Express **13**, 1780 (2005)
17 C.R. Rosberg, D.N. Neshev, A.A. Sukhorukov, W. Krolikowski, Y.S. Kivshar, Opt. Lett. **32**, 397 (2007)
18 O. Peleg, G. Bartal, B. Freedman, O. Manela, M. Segev, D.N. Christodoulides, Phys. Rev. Lett. **98**, 103 901 (2007)
19 A.S. Desyatnikov, D.N. Neshev, Y.S. Kivshar, N. Sagemerten, D. Träger, J. Jägers, C. Denz, Y.V. Kartashov, Opt. Lett. **30**, 869 (2005)
20 A.S. Desyatnikov, N. Sagemerten, R. Fischer, B. Terhalle, D. Träger, D.N. Neshev, A. Dreischuh, C. Denz, W. Krolikowski, Y.S. Kivshar, Opt. Express **14**, 2851 (2006)
21 B. Terhalle, A.S. Desyatnikov, C. Bersch, D. Träger, L. Tang, J. Imbrock, Y.S. Kivshar, C. Denz, Appl. Phys. B **86**, 399 (2007)
22 J. Yang, I. Makasyuk, A. Bezryadina, Z. Chen, Opt. Lett. **29**, 1662 (2004)
23 B. Terhalle, D. Träger, L. Tang, J. Imbrock, C. Denz, Phys. Rev. E **74**, 057 601 (2006)
24 A.A. Zozulya, D.Z. Anderson, A.V. Mamaev, M. Saffman, Phys. Rev. A **57**, 522 (1998)
25 W. Krolikowski, E.A. Ostrovskaya, C. Weilnau, M. Geisser, G. McCarthy, Y.S. Kivshar, C. Denz, B. Luther-Davies, Phys. Rev. Lett. **85**, 1424 (2000)